# Nematic and Smectic Thermotropic Liquid Crystals

**GABRIELA RAU[1], ANCA MIHAELA STOIAN (BULEARCA)[1]*, MANUELA ILEANA PETRESCU[1], DENISA CONSTANTINA AMZOIU[1]**
[1]University of Medicine and Pharmacy of Craiova, Faculty of Pharmacy, 2 Petru Rares Str., 200349, Craiova, Romania

*New azomonoetheramides were synthesized. They were characterized by high melting points and reaction yields. The purity of the new synthesized compounds was verified by a gas chromatograph coupled with a gas spectrometer and it was confirmed by the appearance of a single peak. The synthesized azomonoetheramides were in solid state coloured from yellow to brown, which melt on a temperature range, fact that demonstrated their capability to present nematic and smectic liquid crystals properties. The structural formulas of these compounds were demonstrated by elemental analysis and spectral analysis. Compounds presented smectic phases with monotropic behaviour, presenting the most times polymorphism of the solid phase. In addition, paramorphic nematic phases or with droplets texture and Schlieren texture, respectively, were also put into evidence.*

*Keywords: azomonoetheramides, spectral analysis, droplets, Schlieren, QSAR (Quantitative Structure Activity Relationship)*

Liquid crystals represent a state of matter, having properties between those of a common liquid and those of a solid. In other words, a liquid crystal flows like a liquid, but its molecules are oriented in a crystal-like way [1-3]. Liquid crystals are classified into thermotropic, lyotropic and metallotropic phases. Thermotropic and lyotropic liquid crystals are formed from organic molecules, while the metallotropic ones consist from both organic and inorganic molecules. Only temperature influences the phase transition for thermotropic liquid crystals, both temperature and concentration of liquid crystal molecules in a solvent are responsible for phase transitions in lyotropic liquid crystals, and for metallotropic liquid crystals the influence factors are temperature, concentration and organic-inorganic composition ratio [4-7].

Among other utilizations, liquid crystals have important applications in medicine and pharmaceuticals. Many devices based on liquid crystals are used in areas like spectroscopy, microscopy and imaging, fact that leads to new techniques for optical systems of biological sounding. Biosensors made from liquid crystals allow an unlabelled observation of biological phenomena. Polymers having properties of liquid crystals are used in structures that involve a bio-mimicking for producing colour, in lenses and in elements with muscular action. Liquid crystals are also used in thermographic examination, in the case of diagnostics and monitoring of many diseases, like: diagnosis of cancers, tumours and inflammatory states (liver, lung), evolution of skin tests (allergy), traumatology and forensic medicine [8-10].

In pharmacy, liquid crystals are characterized by their lyotropic state and such based delivery systems are met in creams, gels, ointments, liposomes, colloidal dispersions and transdermal patches with uses in cosmetics and pharmaceuticals. Nafoxidine hydrochloride forms thermotropic and lyotropic liquid crystalline structures, palmitolyl propranolol hydrochloride gives rise smectic type liquid crystalline phase, itraconazole hydrochloride, an antifungal drug, forms chiral nematic phases. Arsphenamine, fenoprofen sodium, fenoprofen calcium, penbutolol sulphate, folic acid, nafcillin, cyclosporine, calcitonin, amylin, nafarelin and leuprolide are other examples of pharmaceutical active compounds capable to display liquid crystalline phases [11-14].

New azomonoetheramides were synthesized through a reaction consisting in condensation in an alkaline medium of some 4-(phenylazo) phenols [15-17], namely: 4-(phenylazo) phenol, more precisely 4-(4'-methyl-phenylazo) phenol and 4-(4'-trifluoromethyl-phenylazo) phenol with 4-ethyl-*N*-chloroacetylaniline (Figure 1).

## Experimental part

### *Materials and methods*

Azophenoxide necessary for reaction is very sensitive to water traces. For this reason, the synthesis of these azomonoetheramides was realized in an anhydrous medium. The synthesis of azomonoetheramides took approximately 5 h. Solid products, coloured from yellow to brown, were obtained. Recrystallization was realized from toluene, and the presence of a single chromatographic peak confirmed the purity of the reaction products.

### *Synthesis of 4'-trifluoromethyl-4-(p-ethyl-N-phenyl-acetamidoxy) azobenzene*

The synthesis was realized in a reflux installation formed by a round-bottomed flask and a reflux condenser in which 0.854 g (2 mmol) 4-(4'- trifluoromethyl) phenol, 0.08 g (2

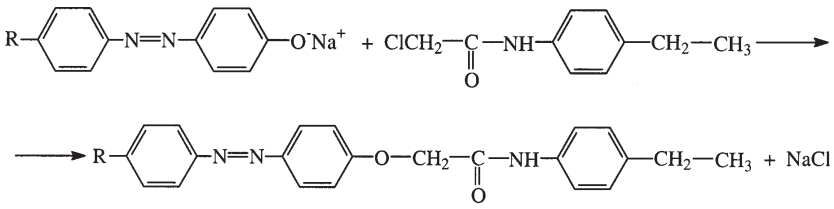


Fig. 1. Synthesis reactions of the new azomonoetheramides

* *email: ancamihaela.stoian@gmail.com*

mmol) NaOH and 10 mL ethanol-benzene mixture (1:1 in volume) were introduced, under stirring. The obtained mixture was maintained under reflux for 2 h, in order to assure the complete reaction of azophenol with sodium hydroxide. Electrical jacket was used as heating source. Then, the reflux condenser was replaced by a distillation one and 3 mL of ethanol-water-benzene azeotropic mixture were distilled. Further, the distillation condenser was replaced by a reflux condenser and 0.363 g (2 mmol) 4-ethyl-*N*-chloroacetylaniline was introduced into the reaction round-bottomed flask. The reaction mixture was homogenized by vigorous stirring, then it was subjected to reflux for more 3 h, at 50–55°C, by the help of the same electrical jacket. After cooling, filtration occurred on a $G_3$ filter. The precipitate was washed well with water directly on the filter in order to remove the sodium chloride and then it was dried in the oven at 105°C. The reaction product was subjected to recrystallization from 50 $cm^3$ toluene. The melting point: 185–186°C. Yield: 80.18%.

The synthesis was similar for all novel azomonoetheramides.

*Reagents*

All substances necessary for the synthesis of the new azomonoetheramides were Fluka or Merck commercially available products.

*Equipments*

The melting points were established with a Boetius apparatus and a Sanyo apparatus. Elemental analysis was made on CHNOS Vario El analyzer. Electronic spectra were recorded with a UV–Vis Jasco V–530 spectrophotometer, within 200–700 nm range. Dioxane solutions ($4\times10^{-5}$ M) were prepared one day before recording spectra and kept in a dark place. FTIR spectra were recorded in potassium bromide pellets (KBr, Merck), with a Bio-Rad FTS 135 spectrophotometer, within the range 3500–400 $cm^{-1}$. Mass spectra were obtained using a HPGC–MS 5890 MD 5971 spectrometer, at 70 eV, with carrier gas He at 2 mL/min. The $^1$H–NMR spectra were recorded with a Varian NMR-System 300 spectrometer, at 300 MHz, in DMSO–$d_6$. The chemical shifts referred to tetramethylsilane (TMS) as internal standard.

Phase sequences and phase transition temperatures were determined by *polarizing optical microscopy (POM)* – it was applied using an IOR MC–5A polarized light microscope with a heating table at 10°C/min rate for both heating and cooling, and *differential scanning calorimetry (DSC)* –the compounds were analyzed with a Perkin Elmer DSC–2 device with the same heating–cooling rate (10°C/min.). To separate the transition peaks, sometimes the study was carried out at lower speeds (5°C/min, 2°C/min). The device was set at 5 mcal/s sensitivity, in an inert atmosphere of argon.

## Results and discussions

Reaction yields are dependent on the reaction products solubility in toluene. The high melting points are due to the presence of different substituents in the *para* position (table 1).

*UV–Vis spectra*

The bands of benzene E or B type are due to conjugation of the π electrons from the benzene rings and they gave absorption bands of medium intensity at 240–271 nm. The bands of K type, due to the conjugated Ar–N=N–Ar system, presented absorption bands intense at 347–369 nm, and the R type bands, characteristic to the –N=N– chromophoric group, gave absorption bands of weak intensity, of R type at 438–445 nm.

The elemental analysis results (C, H, N), the wave lengths at which the maximum absorptions occurred and the extinction molar coefficients are presented in table 2.

| No. | Structural formulas | Molecular formulas | M | M.p. [°C] | η [%] |
|---|---|---|---|---|---|
| 1. | 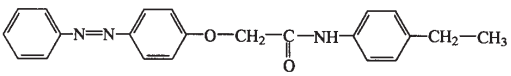 4-(*p*-ethyl-*N*-phenylacetamidoxy) azobenzene | $C_{22}H_{21}N_3O_2$ | 359 | 197–198 | 75.26 |
| 2. | 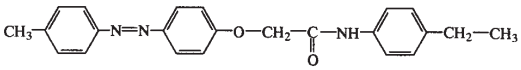 4'-methyl-4-(*p*-ethyl-*N*-phenylacetamidoxy) azobenzene | $C_{23}H_{23}N_3O_2$ | 373 | 191–192 | 70.72 |
| 3. | 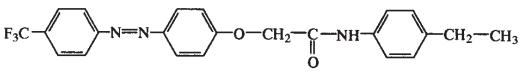 4'-trifluoromethyl-4-(*p*-ethyl-*N*-phenylacetamidoxy) azobenzene | $C_{23}H_{20}N_3O_2F_3$ | 427 | 185–186 | 80.18 |

**Table 1**
STRUCTURAL FORMULAS, MOLECULAR MASSES, MELTING POINTS AND YIELDS FOR THE NOVEL SYNTHESIZED COMPOUNDS

| No. | Structural formulas | $\lambda_{max}$ [nm] | $\varepsilon_{max}$ [1000 $cm^2$] / mol | Elemental analysis %C *calcd.* / *found* | %H *calcd.* / *found* | %N *calcd.* / *found* |
|---|---|---|---|---|---|---|
| 1. | 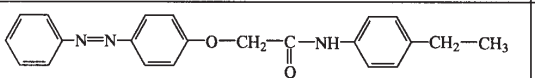 4-(*p*-ethyl-*N*-phenylacetamidoxy) azobenzene | 266<br>347<br>445 | 19396<br>48860<br>3385 | 73.53<br>73.20 | 5.84<br>5.61 | 11.69<br>11.12 |
| 2. | 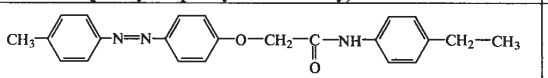 4'-methyl-4-(*p*-ethyl-*N*-phenylacetamidoxy) azobenzene | 271<br>355<br>438 | 9869<br>34754<br>3389 | 73.99<br>73.61 | 6.16<br>6.00 | 11.26<br>11.09 |
| 3. | 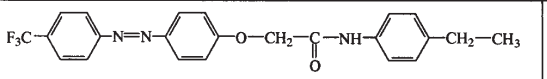 4'-trifluoromethyl-4-(*p*-ethyl-*N*-phenylacetamidoxy) azobenzene | 252<br>349<br>444 | 80977<br>11282<br>3227 | 64.63<br>64.65 | 4.68<br>4.70 | 9.83<br>9.90 |

*calcd.* – Calculated.

**Table 2**
UV–Vis ABSORPTION BANDS AND ELEMENTAL ANALYSIS OF THE NOVEL COMPOUNDS

| No. | Structural formulas | FTIR absorption bands, $\nu$ [cm$^{-1}$] | | | | |
|---|---|---|---|---|---|---|
| | | -N=N- | -NH- | $C_{Ar}$–O–$CH_2$– *antisym.* | *sym.* | –CO–NH– *amide I/ amide II* |
| 1. | 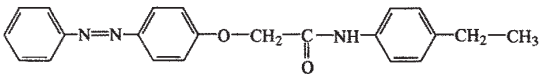 4-(*p*-ethyl-*N*-phenylacetamidoxy) azobenzene | 1431 (s) | 3379 (s) | 1258 (fi) | 1060 (i) | 1680 (fi) 1539 (i) |
| 2. | 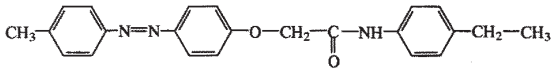 4'-methyl-4-(*p*-ethyl-*N*-phenylacetamidoxy) azobenzene | 1438 (s) | 3385 (s) | 1253 (fi) | 1062 (i) | 1679 (fi) 1541 (i) |
| 3. | 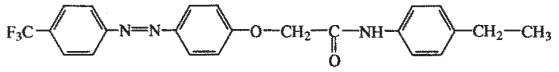 4'-trifluoromethyl-4-(*p*-ethyl-*N*-phenylacetamidoxy) azobenzene | 1439 (s) | 3390 (s) | 1250 (fi) | 1066 (i–fi) | 1682 (fi) 1529 (i) |

FTIR absorption bands: *vi* – Very intense; *i* – Intense; *m* – Moderate; *w* – Weak; *antisym.* – Anti-symmetric; *sym.* – Symmetric.

**Table 3**
FTIR ABSORPTION BANDS OF THE COMPOUNDS

| No. | Aromatic protons | NH | $CH_2$ (-O-$CH_2$-) | $CH_3$ ($CH_3$-Ar) | $CH_2$ (-$CH_2$-$CH_3$) | $CH_3$ (-$CH_2$-$CH_3$) |
|---|---|---|---|---|---|---|
| 1. | 7.4 m | 8.2 s | 4.9 s | – | 2.4 q | 1.3 t |
| 2. | 7.5 m | 8.2 s | 4.9 s | 2.4 s | 2.6 q | 1.2 t |
| 3. | 7.4 m | 8.3 s | 4.8 s | – | 2.5q | 1.2 t |

*m* – multiplet; *s* – singlet; *t* – triplet, *q* – quartet.

**Table 4**
$^1$H–NMR DATA OF THE NOVEL COMPOUNDS

*FTIR spectra*

An important band from spectrum was the one of the $\nu_{CO}$ valence vibration of the amide group, so-called **amide I**, which appeared at 1682–1679 cm$^{-1}$. The usually most intense band from the spectrum, which was registered at 1541–1529 cm$^{-1}$, was considered to be the **amide II** band (table 3).

The band due to $\nu_{N=N}$ valence vibration should have been characteristic, but, due to the fact that the bond polarity was very weak, the absorptions were produced at small values of the wave lengths and the bands had low intensities (1439–1431 cm$^{-1}$).

As it was observed from the structure of the new compounds, they all had $CH_2$ and $CH_3$ groups, and thus they presented absorption bands in the zone of aliphatic radicals, namely anti-symmetric $\nu_{CH3}$ valence vibrations and anti-symmetric $\nu_{CH2}$ valence vibrations.

*$^1$H-NMR spectra.* In the $^1$H-NMR spectra of (1) and (3) compounds, five signals appeared, from which a multiplet characteristic to aromatic protons at δ(ppm) = 7.4–7.5, two uncleaved signals, singlet, given by the protons from the NH (δ(ppm) = 8.2–8.3) and $CH_2$ (–O–$CH_2$–, δ(ppm) = 4.8–4.9) groups, two cleaved signals: a quartet signal given by the protons from the $CH_2$ group (–$CH_2$–$CH_3$, δ(ppm) = 2.4–2.6) and a triplet signal given by the protons from the $CH_3$ group (–$CH_2$–$CH_3$, δ(ppm) = 1.2–1.3).

For 4'-methyl-4-(*p*-ethyl-N-phenylacetamidoxy) azobenzene (2), five signals also appeared, but this compound was characterized by a singlet given by the protons from the $CH_3$ group ($CH_3$–Ar, δ(ppm) = 2.4) (table 4).

*Aromatic azomonoetheramides as new organic materials for nonlinear optics*

4-(*p*-ethyl-*N*-phenylacetamidoxy) azobenzene (1) presented a narrow range of temperatures of existence for the nematic phase at cooling. Isotropic-nematic liquid transition was put into evidence only at a low cooling rate of 2°C/min, when the transition peak from the DSC diagram (fig. 2) was separated from the peak of crystallization. The appearance of the nematic phase (fig. 3), instead of smectic phase from the compound (2) having a methyl substituent, demonstrated the rule of depression of the smectic phase by the more bulky group laterally attached.

4'-methyl-4-(*p*-ethyl-*N*-phenylacetamidoxy) azobenzene (2) presented a polymorphism of solid phase at heating, while at cooling a nematic phase, followed by a smectic A phase. From the DSC diagram (fig. 4), the following succession of phases at cooling was observed:

– I 191 N 189.25 $S_A$ 176.15 $K_1$ 164.85 K (I - isotropic liquid, N - nematic phase, $S_A$ - smectic A phase, K, $K_1$ - crystalline phase).

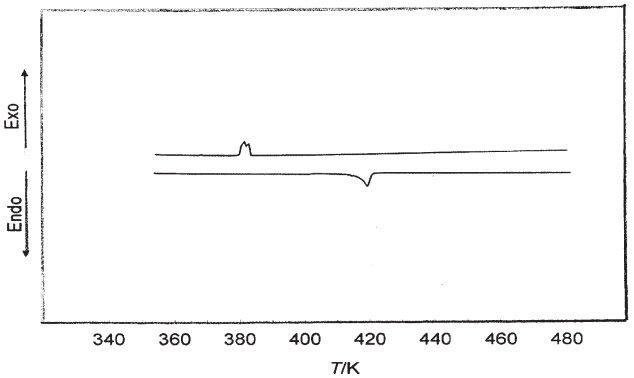


Fig. 2. DSC diagram of 4-(*p*-ethyl-*N*-phenylacetamidoxy) azobenzene (1)

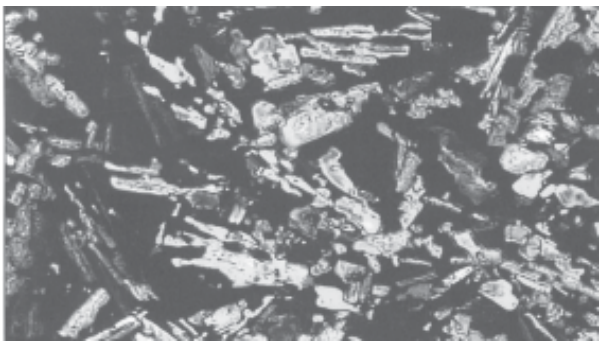

Fig. 3. Appearance of the nematic phase from the isotropic liquid at cooling.

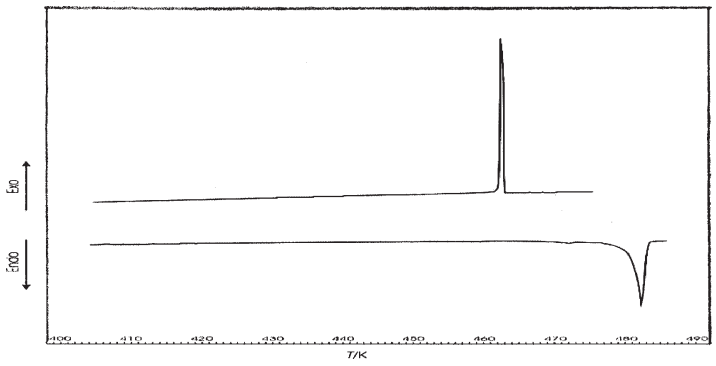


Fig. 4. DSC diagram of 4'-methyl-4-(*p*-ethyl-*N*-phenylacetamidoxy) azobenzene (2).

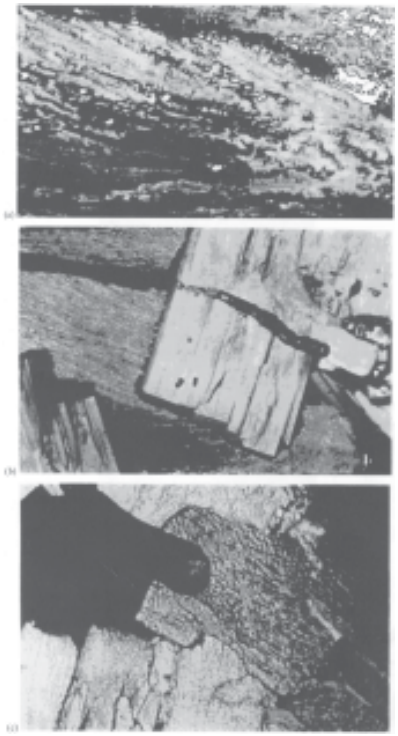

Fig. 5. Textures of (a) solid, (b) smectic and (c) nematic phases.

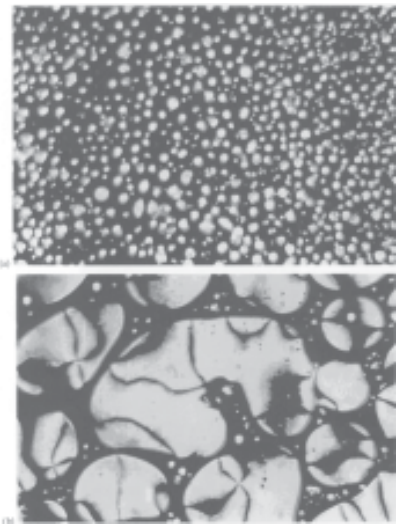

Fig. 6. Nematic mesophase, characterized by the so-called *droplets* texture (a), *Schlieren* texture (b).

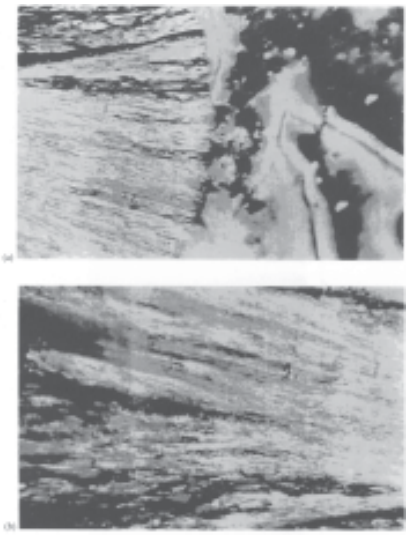

Fig. 7. Phase transition nematic-smectic (a), phase characterized by the fan texture (b).

Figures 5a, 5b and 5c were realized when heating the compound (2) and represented the textures from solid, smectic and nematic phases. The nematic mesophase appeared when cooling the compound. It was characterized by the so-called *droplets* texture (fig. 6a), which was transformed into the *Schlieren* texture (fig. 6b) with the temperature decreasing. The nematic-smectic phase transition was observed in the figure 7a. This phase was characterized by the fan texture (fig. 7b).

4'-trifluoromethyl-4-(*p*-ethyl-*N*-phenylacetamidoxy) azobenzene (3) presented a smectic A phase, on a very narrowed domain, and a paramorphic nematic phase, at heating. Additionally, it was observed a slightly exothermal behaviour, due to the elevated thermal dilatation coefficient. This characteristic was specific to the majority of compounds having trifluoromethyl as substituent. The succession of phases in the case of this compound, observed by microscopy in polarized light and confirmed by the help of DSC diagrams (fig. 8), is the following:

– K 185 $K_1$ 165.35 $S_A$ 155.25 N 144 I at first heating-cooling cycle (I - isotropic liquid, N - nematic phase, K, $K_1$ - crystalline phase).

Figure 9 showed the appearance of the texture for paramorphic smectic phase from the solid phase, at heating. At a very slowly cooling (under 5°C/min), isotropic-nematic transition peaks appeared, and at lower temperatures the nematic-smectic A transition. Thus, the enantiotropic character of the substance was highlighted.

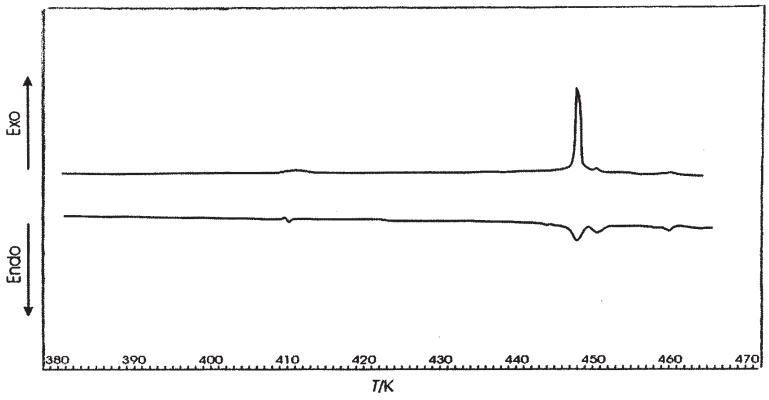


Fig. 8. DSC diagram of 4'-trifluoromethyl-4-(*p*-ethyl-*N*-phenylacetamidoxy) azobenzene (3).

| $R^2$ | $x_i$ |
|---|---|
| 0.4673 | 71 |
| 0.4307 | 268 |
| 0.5991 | 71; 126 |
| 0.5777 | 71; 82 |

**Table 5**
THE BEST CORRELATIONS Temp = $f(x_i)$

71. Average atomic electrophilic reaction index for a C atom; 126. RNCS Relative negative charged SA; 82. Max atomic one–electron reaction index for a N atom; 268. Min electron–electron repulsion for a C–H bond.

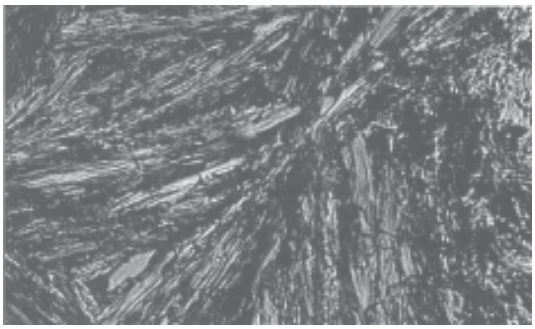

Fig. 9. Paramorphic smectic phase.

*Structure–property correlation (QSAR/QSPR)*

Correlation of melting points of the new synthesised azomonoetheramides, having the chemical structures represented by different structural properties, generically called descriptors (electrostatic, topological, thermodynamic or cuanto-molecular), which represented the chemical structures, demonstrated that they are in fact an interface between the actual chemical structures and the studied physico-chemical property. The procedure of statistical correlation between these molecular descriptors and property was realized by multiple linear regressions and it is called QSAR (Quantitative Structure Activity Relationship) or QSPR (Quantitative Structure Property Relationship) [18].

Molecular descriptors representing the studied chemical structures were obtained using the following programs:

- molecular modeling of chemical structures for the studied substances was realized with Hyperchem 6.0 (trial version) program, using the $MM^+$ (Molecular Mechanics) method;

- cuanto-molecular computations of molecular geometries were performed using the program pack MOPAC 6.0 that comprises a series of semi empirical approximations of RHF (Restricted Hartree Fock) type calculus. PM 3 (Parameter Model 3) procedure was utilized for the semi empirical parameters used in quantum computations of molecular structures;

- estimation of molecular descriptors and structure-property correlation (melting points) of the studied substances were done by the help of CODESSA 2.1 program.

The obtained results were given in table 5.

As it seen from the table 5, among all molecular descriptors that have a significant contribution ($R^2$ = 0.4673) for melting points, the 71 descriptor seemed to be relevant, in combination with the 126 descriptor ($R^2$ = 0.5911) or in combination with the 82 descriptor ($R^2$ = 0.5777), namely the monoelectronic reaction index for the nitrogen atoms. The high enough values of the $R^2$ correlation coefficients showed the contribution of these structural measures to setting the melting point property. The fact that $R^2$ is not closed to unity demonstrated that other factors of macroscopic nature also participated when setting the melting point.

## Conclusions

The synthesised azomonoetheramides were physico-chemical characterized, namely: melting point, elemental analysis, UV-VIS, FTIR, mass and $^1$H-NMR spectral analysis.

The study of properties for nematic and smectic liquid crystals demonstrated that the size, position and the terminal group polarity had a strong influence on both the type of the mesophase presented by a certain compound and the transition temperatures. The statistical correlation between the melting points for the synthesized azomonoetheramides and the chemical structures was performed by different structural properties, generically called descriptors. Multiple linear regressions named QSAR (Quantitative Structure Activity Relationship) or QSPR (Quantitative Structure Property Relationship) were used.

## References


1. RAI, G., JAIN, D., Int. J. Pharma. Sci. Rev. Res., **4**, no. 2, 2010, p. 129-134.
2. CASTELLANO, J.A., published in World Scientific Publishing, Liquid Gold: The Story of Liquid Crystal Displays and the Creation of an Industry, 2005.
3. ANDRIENKO, D., published in International Max Planck research school modelling of soft matter, Introduction to liquid crystals, 2006, Bad Marienberg, p. 27-29.
4. CRAWFORD, G.P., WOLTMAN, S.J., published in World Scientific Publishing Co. Pte. Ltd., Liquid crystals: frontiers in biomedical applications, 2007, chapter 1.
5. TIETZ, J.I., MASTRIANA, J.R., SAMPSON, P., SEED, A.J., Liq. Cryst., **39**, 2012, p. 515–530.
6. HONGLAWAN, A., BELLER, D.A., CAVALLARO, M., KAMIEN, R.D., STEBE, K.J., YANG, S., Proceed. Nat. Acad. Sci., **110**, 2013, p. 34-39.
7. KIM, B.G., JEONG, E.J., CHUNG, J.W., SEO, S., KOO, B., KIM, J., Nat. Mater., **12**, 2013, p. 659–664, doi:10.1038/nmat3595.
8. STASIEK, J., STASIEK, A., JEWARTOWSKI, M., COLLINS, M.W., Opt. & Laser Technol., **38**, no. 4, 2006, p. 243-256, http://dx.doi.org/10.1016/j.optlastec.2005.06.028.
9. STASIEK, J., JEWARTOWSKI, M., KOWALEWSKI, T.A., J. Crystall. Process Technol., **4**, 2014, p. 46-59, http://dx.doi.org/10.4236/jcpt.2014.41007.
10. TKACHENKO, G.V., TKACHENKO, V., ABBATE, G., published in InTech publisher under CC BY-NC-SA 3.0 license, Tkachenko GV (Ed): New developments in liquid crystals, 2009, chapter 1.
11. KENT STATE UNIVERSITY, New Drug Paradigm: Liquid Crystal Pharmaceuticals, ScienceDaily, 2007, <www.sciencedaily.com/releases/2007/09/070906135516.htm>.
12. GAIKWAD, P.P., DESAI, M.T., Int. J. Pharma Res. & Rev., **2**, no. 12, 2013, p. 40-52.
13. BUNJES, H., RADES, T., J. Pharma. Pharmacol., **57**, 2005, p. 807-816, DOI 10.1211/0022357056208, ISSN 0022-3573.
14. CHEN, Y., MA, P., GUI, S., BioMed Res. Int., **2014**, 2014, article ID 815981, 12 pages, http://dx.doi.org/10.1155/2014/815981.
15. RĂU, G., MOGOŞANU, G.D., PISOSCHI, C.G., STĂNCIULESCU, C.E., Farmacia, **62**, no. 3, 2014, p. 486–495.
16. RADU, S., RĂU, G., MOANŢĂ, A., Rev. Chim. (Bucharest), **52**, 2001, p. 619
17. RĂU, G., AMZOIU, D.C., STOIAN (BULEARCĂ), A.M., STĂNCIULESCU, C.E., PISOSCHI, C.G., Rev. Chim. (Bucharest), **66**, no. 1, 2015, p. 131
18. KARELSON, M., LOBANOV, V.S., Chem. Rev., **96**, 1996, p. 1027–1043.


Manuscript received: 26.01.2015